

Effect of transversal concentration gradient on H_2-O_2 cellular detonation

Cheng Wang(王成), Yi-Xuan Wu(吴易烜), Jin Huang(黄金), Wen-Hu Han(韩文虎), Qing-Guan Song(宋清官)

Citation: Chin. Phys. B . 2020, 29(6): 060503 . **doi:** 10.1088/1674-1056/ab81f5
Journal homepage: http://cpb.iphy.ac.cn; http://iopscience.iop.org/cpb

What follows is a list of articles you may be interested in

Fluctuation theorem for entropy production at strong coupling

Y Y Xu(徐酉阳), J Liu(刘娟), M Feng(冯芒)

Chin. Phys. B . 2020, 29(1): 010501 . **doi:** 10.1088/1674-1056/ab592d

The heat and work of quantum thermodynamic processes with quantum coherence

Shanhe Su(苏山河), Jinfu Chen(陈劲夫), Yuhan Ma(马宇翰), Jincan Chen(陈金灿), Changpu Sun(孙昌璞)

Chin. Phys. B . 2018, 27(6): 060502 . **doi:** 10.1088/1674-1056/27/6/060502

Relating Maxwell's demon and quantitative analysis of information leakage for practical imperative programs

Kushal Anjaria, Arun Mishra

Chin. Phys. B . 2017, 26(10): 100507 . **doi:** 10.1088/1674-1056/26/10/100507

Analysis of the induction of the myelin basic protein binding to the plasma membrane phospholipid monolayer

Lei Zhang(张蕾), Changchun Hao(郝长春), Ying Feng(冯盈), Feng Gao(高峰), Xiaolong Lu(逯晓龙), Junhua Li(李俊花), Runguang Sun(孙润广)

Chin. Phys. B . 2016, 25(9): 090507 . **doi:** 10.1088/1674-1056/25/9/090507

Behavior of lysozyme adsorbed onto biological liquid crystal lipid monolayer at the air/water interface

Xiaolong Lu(逯晓龙), Ruixin Shi(史瑞新), Changchun Hao(郝长春), Huan Chen(陈欢), Lei Zhang(张蕾), Junhua Li(李俊花), Guoqing Xu(徐国庆), Runguang Sun(孙润广)

Chin. Phys. B . 2016, 25(9): 090506 . **doi:** 10.1088/1674-1056/25/9/090506

Effect of transversal concentration gradient on H_2–O_2 cellular detonation*

Cheng Wang(王成)[1], Yi-Xuan Wu(吴易烜)[1], Jin Huang(黄金)[1,†], Wen-Hu Han(韩文虎)[1], and Qing-Guan Song(宋清官)[2]

[1] *State Key Laboratory of Explosion Science and Technology, Beijing Institute of Technology, Beijing* 100081, *China*
[2] *Institute of Chemical Materials, China Academy of Engineering Physics, Mianyang* 621900, *China*

(Received 18 November 2019; revised manuscript received 9 March 2020; accepted manuscript online 23 March 2020)

A two-dimensional detonation in H_2–O_2 system is simulated by a high-resolution code based on the fifth-order weighted essentially non-oscillatory (WENO) scheme in the spatial discretization and the 3th-order additive Runge–Kutta schemes in the time discretization, by using a detailed chemical model. The effect of a concentration gradient on cellular detonation is investigated. The results show that with the increase of the concentration gradient, the cell instability of detonation increases and gives rise to the oscillation of average detonation velocity. After a long time, for the case of the lower gradient the detonation can be sustained, with the multi-head mode and single-head mode alternating, while for the higher gradient it propagates with a single-head mode.

Keywords: detonation, detailed reaction, WENO, additive Runge–Kutta (ARK), concentration gradient

PACS: 05.70.–a, 45.20.dh, 47.10.ad, 47.40.Rs **DOI:** 10.1088/1674-1056/ab81f5

1. Introduction

Since detonations often take place and propagate in the non-homogeneous mixtures, the investigating of the detonation behavior in non-uniform mixtures is significant not only for the industrial explosion in the leakage combustible gas, but also for the experimental investigations with a vertical concentration gradient caused by the difference in the molecular weight of gas mixture.[1]

It is well established that while detonation waves are inherently unstable and possess a multi-dimensional and cellular structure in a uniform medium, globally they maintain a steady average velocity that is remarkably close to the Chapman–Jouguet (CJ) velocity. Short and Sharpe[2,3] studied the detonation instability through conducting numerical solutions and predicting unstable solutions for the nonlinear dynamics such as increasing exothermicity. Ng *et al.*[4] then extended the work of Short and Sharpe[2] by carrying out a series of numerical computations and introducing a well-defined quantitative parameter to characterize the one-dimensional detonation stability. Recently, Zhang *et al.*[5] experimentally studied the instabilities of detonation[6] in uniform media and discussed the effects of detonation instability on the propagation modes near the limits in typical combustible mixtures and assessed the role of induction length on the near-limit detonation.[7] Previous studies[8–12] indicated that the detonations propagating in nonhomogeneous media differed significantly from those in uniform mixtures, taking on two kinds of detonation behaviors determined by inhomogeneity. Thomas, *et al.*[13] discussed the influence of concentration gradient parallel to pipeline axis on detonation propagation and observed the quenching and reinitiating behaviors for different concentration gradients, which was also analyzed by Vidal.[14] Oran *et al.*[15] have found that there existed complicated shock structures on the interface between hydrogen and oxygen mixture. The detonation with concertation gradient perpendicular to propagating direction was investigated.[16] Kessler *et al.*[17] found experimentally that a detonation has a bended front in a non-uniform ethylene–oxygen mixture. Boeck *et al.*[18] displayed experimentally the cell pattern of H_2-air detonation with transverse concentration gradient by using soot foils, and found that concentration gradient gives rise to the changes of cell pattern and the deficit of detonation velocity. Ishii and Kojima,[12,19] found that the detonation is inclined in fuel-lean H_2–O_2 and H_2–O_2–N_2 mixtures with transverse concentration gradient. Calhoon and Sinha[20] presented numerically the triple-shock structure of two-dimensional detonation by using one-step reaction model and setting an inflow boundary with a hyperbolic tangent function, showing that concentration gradient triggers the cellular instability of detonation and results in the transition from the cell pattern to another. Kessler, Gamezo and Oran[21] studied the detonation propagations in nonhomogeneous media by using a calibrated single-step reaction model to embody the gradient of mixture composition. Although detonations in non-uniform media have been simulated previously,[22–32] the used model is still a one-step reaction

*Project supported by the Natural National Science Foundation of China (Grant Nos. 11972090, 11732003, and U1830139), the Beijing Natural Science Foundation, China (Grant No. 8182050), and the National Key Research and Development Program of China (Grant No. 2017YFC0804700).

†Corresponding author. E-mail: huangjin@bit.edu.cn

© 2020 Chinese Physical Society and IOP Publishing Ltd

model and concentration gradient cannot be really formed by changing composition of fuel and oxygen. Consequently, detonation propagations in the nonhomogeneous media cannot be revealed due to the lack of real chemistry.

Recognizing that detonation in non-uniform medium depends strongly on real chemistry and its study is still rare, a two-dimensional detonation with transversal concentration gradient is undertaken by using the detailed reaction mechanism. Objectives of the study are to show the detonation behaviors for different concentration gradients. We first present the multi-species reactive Euler equations, and then give their results and discussion.

2. Governing equations

Reactive flow Euler equations are used to describe the detonation propagation in an H_2–O_2 system with multispecies and detailed reactions as follows:

$$\frac{\partial \boldsymbol{U}}{\partial t}+\frac{\partial \boldsymbol{F}(\boldsymbol{U})}{\partial x}+\frac{\partial \boldsymbol{G}(\boldsymbol{U})}{\partial y}=\boldsymbol{S}(\boldsymbol{U}), \tag{1}$$

$$\boldsymbol{U}=\begin{pmatrix}\rho\\ \rho u\\ \rho v\\ \rho e\\ \rho Y_1\\ \vdots\\ \rho Y_{N-1}\end{pmatrix},\quad \boldsymbol{F}(\boldsymbol{U})=\begin{pmatrix}\rho u\\ \rho u^2+p\\ \rho uv\\ \rho u(e+p/\rho)\\ \rho uY_1\\ \vdots\\ \rho uY_{N-1}\end{pmatrix},$$

$$\boldsymbol{G}(\boldsymbol{U})=\begin{pmatrix}\rho v\\ \rho vu\\ \rho v^2+p\\ \rho v(e+p/\rho)\\ \rho vY_1\\ \vdots\\ \rho vY_{N-1}\end{pmatrix},\quad \boldsymbol{S}(\boldsymbol{U})=\begin{pmatrix}0\\ 0\\ 0\\ 0\\ \dot{\omega}_1\\ \vdots\\ \dot{\omega}_{N-1}\end{pmatrix}, \tag{2}$$

$$e=h-\frac{p}{\rho}+\frac{(u^2+v^2)}{2}, \tag{3}$$

$$p=\rho RT, \tag{4}$$

where p, ρ, e, T, u, v, and h are the pressure, density, total energy of unit mass, temperature, x- and y-direction velocity and enthalpy of unit mass; $Y_1\cdots Y_{N-1}$ are mass fraction of species in detailed chemical kinetics model, where $\sum_{i=1}^{N} Y_i=1$; R is the universal gas constant.

The species involving chemical reaction are H_2, O_2, OH, O, H, H_2O_2, HO_2, and H_2O. Reaction equations can be unified into the following form:

$$\sum_{i=1}^{N}\upsilon'_{mi}X_i \underset{kb_m}{\overset{kf_m}{\rightleftharpoons}} \sum_{i=1}^{N}\upsilon''_{mi}X_i,\quad m=1,2,3,\ldots,20, \tag{5}$$

where υ'_{mi} and υ''_{mi} are the chemical stoichiometric reactant and product of the i-th species in the m-th reaction; X_i is the mole fraction of the i-th species; kf_m and kb_m are the forward and backward reaction-rate constants of the m-th reaction, which can be calculated from the following formulae:

$$\begin{cases} kf_m=A_mT^{nm}\exp\left(-\dfrac{Ea_m}{R_0T}\right),\\ kp_m=\exp\left\{\sum\limits_{i=1}^{N}\left[(\upsilon''_{mi}-\upsilon'_{mi})\left(\dfrac{s_i^0}{R_i}-\dfrac{h_i}{R_iT}\right)\right]\right\},\\ ke_m=kp_m\left(\dfrac{p_0}{R_0T}\right)^{\sum\limits_{i=1}^{N}(\upsilon''_{mi}-\upsilon'_{mi})},\\ kb_m=\dfrac{kf_m}{ke_m}. \end{cases} \tag{6}$$

Here, A_m, n_m, and Ea_m are the pre-exponential constant, the temperature power, and the activation energy, respectively; R_i, s_i^0, and h_i are the universal gas constant, the entropy at the standard state, and the specific enthalpy of the i-th species; p_0 is the atmospheric pressure. In summary, the density production rate of the i-th species, $\dot{\omega}_i$, is

$$\begin{aligned}\dot{\omega}_i=\ & W_i\sum_{m=1}^{20}(\upsilon''_{mi}-\upsilon'_{mi})\times \mathrm{TB}\\ &\times\left(kf_m\prod_{i=1}^{N}\left(\frac{\rho_i}{W_i}\right)^{\upsilon'_{mi}}-kb_m\prod_{i=1}^{N}\left(\frac{\rho_i}{W_i}\right)^{\upsilon''_{mi}}\right),\end{aligned} \tag{7}$$

where TB is the index of the third body effect.

$$\mathrm{TB}=\begin{cases}1, & \text{no third body effect},\\ \sum\limits_{i=1}^{N}\alpha_{mi}\dfrac{\rho_i}{W_i}, & \text{third body effect},\end{cases} \tag{8}$$

where α_{mi} is the third body effect coefficient.

3. Results and discussion

3.1. Calculation model and initial conditions

The channel width and length are respectively 36 mm and 220 mm. The channel is filled with H_2–O_2 mixture. The left side is the inlet, and the right side is the outflow. A resulting cellular detonation is set to be an initiation zone at the left as shown in Fig. 1; in the rest, the gas is stationary and its initial pressure and temperature are 6.67 kPa and 298 K, respectively.



Fig. 1. Calculation model: cellular detonation propagates rightward; transverse concentration gradient is set to be produced in unreacted gas.

To study systematically the influence of concentration gradient on detonation, eleven cases are selected to to be simulated as shown in Table 1. The concentration is linearly distributed from the lower to the upper, and therefore the mixture has a transition from the poor fuel to the rich fuel.

Table 1. Mass fraction of Y_{H_2} and Y_{O_2} on lower and upper walls, where φ is equivalence ratio of concentration; Y_{H_2} and Y_{O_2} are mass fractions of H_2 and O_2, respectively.

Case	Lower wall			Upper wall		
	φ	Y_{H_2}	Y_{O_2}	φ	Y_{H_2}	Y_{O_2}
1	1.0	0.111	0.889	1.0	0.111	0.889
2	0.9	0.101	0.899	1.1	0.121	0.879
3	0.8	0.091	0.909	1.2	0.130	0.870
4	0.7	0.080	0.920	1.3	0.140	0.860
5	0.6	0.070	0.930	1.4	0.149	0.851
6	0.5	0.059	0.941	1.5	0.158	0.842
7	0.4	0.048	0.952	1.6	0.167	0.833
8	0.3	0.036	0.964	1.7	0.175	0.825
9	0.2	0.024	0.976	1.8	0.184	0.816
10	0.1	0.012	0.988	1.9	0.192	0.808
11	0	0	1.0	2.0	0.2	0.8

3.2. Effects of concentration gradient on frontal structure of detonation

Figure 2 shows the cell evolution and frontal structure of detonation for the case. The transverse wave structure can be seen in Fig. 2(a), and triple points are formed by the collision of transverse wave structure. Furthermore, the number of triple points is 8 and keeps constant in the detonation propagation. The trajectory of the triple point constructs a detonation cell as shown in Fig. 2(b). The cellular structure takes a scaly structure with basically uniform cell size.

By steepening concentration gradient, detonation structure in a nonhomogeneous medium continues to increases the irregularity of detonation cell, which is also consistent with that presented by Austin *et al.*[33] For the weakly irregular detonation, we mainly take the case 4 as a typical example. Figure 3 shows the pressure, the temperature, and the OH mass fraction contours at different times. It is seen clearly that the triple points appear on the detonation front and the number of triple points can be constant and consequently detonation can be sustained.

Figure 4 shows the history of shock pressure along the upper and lower walls. It is observed that the shock pressure profiles on the upper and lower wall take on a quasi-periodic oscillation with the same period. The peak pressure on the upper wall is ~ 0.9 MPa higher than the Von-Neumann value, while that on the lower wall is ~ 0.4 MPa, which is twice higher than the Von-Neumann value. Consequently, the peak pressure along the upper wall is obviously higher than on the lower wall. The transversal concentration gradient gives rise to the difference between average detonation velocities in fuel-lean and fuel-rich layers and consequently leading the detonation front to incline relative to the vertical direction (see Fig. 3). An inclination degree can be defined by calculating an angle between a detonation front and the vertical direction. Figure 5 shows the change of inclination angle with time for the cases 2–4. It is seen that for the case 2 the inclination angle initially increases and then oscillates around a certain value. For cases 3 and 4, the characteristics are similar to those in case 2 and the inclination angle is $\sim 3.1^\circ$ for the case 3 and $\sim 5.0^\circ$ for the case 4. It is seen further that the averaged angle increases as the transversal concentration gradient augments. For the cases 2–4, a Mach reflection at the lower wall appears as the inclination angle does not reach the critical value for a regular reflection.[1]

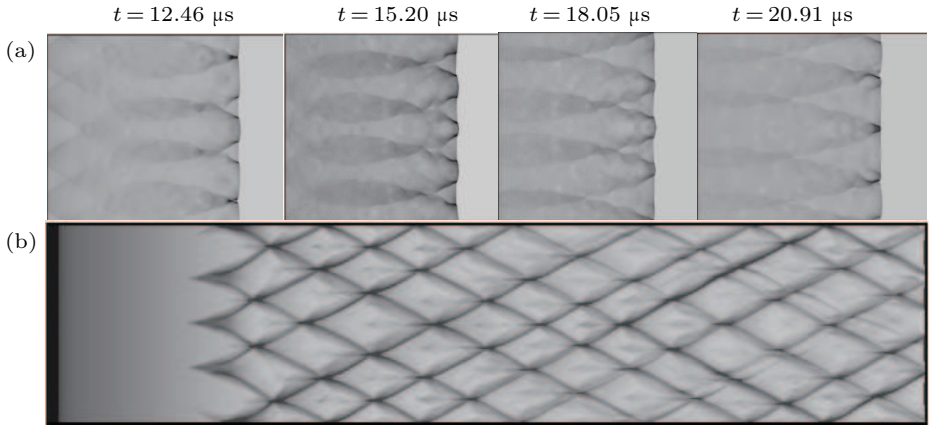


Fig. 2. Frontal structure of detonation front at different times and detonation cell: (a) pressure contours; (b) maximum pressure histories.

In summary, for a lower transverse concentration gradient, a detonation feature is globally similar to that in the uniform mixture, with the multi-head structure on the front.

For the mildly irregular detonation, the case 6 is selected as an object to be discussed. Figure 6 shows the pressure, temperature and OH mass fraction contours near the detonation wave front at different times. Initially, the detonation is similar to that in the case 4. At $t = 11.27$ μs, the detonation front inclines obviously, with triple-shock structure shown in Fig. 6(a). As the detonation propagates, the inclination angle becomes larger. At $t = 29.52$ μs, Mach reflection in the fuel-rich layer near the

upper wall occurs and results in locally strong explosion due to high heat release, where overdriven detonation produces and fast advances with strong Mach shock. However, the detonation near fuel-lean layer is relatively regular and sustained through triple-point collision as shown in Figs. 6(b) and 6(c). It is seen further that OH mass fraction behind the Mach shock is low and mainly gathers at the location of the triple-point collision and in the fuel-lean layer, see Fig. 6(c). Figure 7 shows the history of the maximum pressure along the upper and lower walls. It is seen that pressure pulse at the upper wall is of large-amplitude and low-frequency, while at the lower wall it is of small-amplitude and high-frequency pressure. The peak pressure at the upper wall increases up to ~ 1.55 MPa, which is much higher than that at the lower wall, ~ 0.57 MPa. Furthermore, the global inclination angle increases and reaches a critical angle as the concentration gradient increases, and therefore the Mach reflection occurs at the lower wall, leading the peak pressure at upper wall and lower wall to obviously increase relative to that in the case 4.

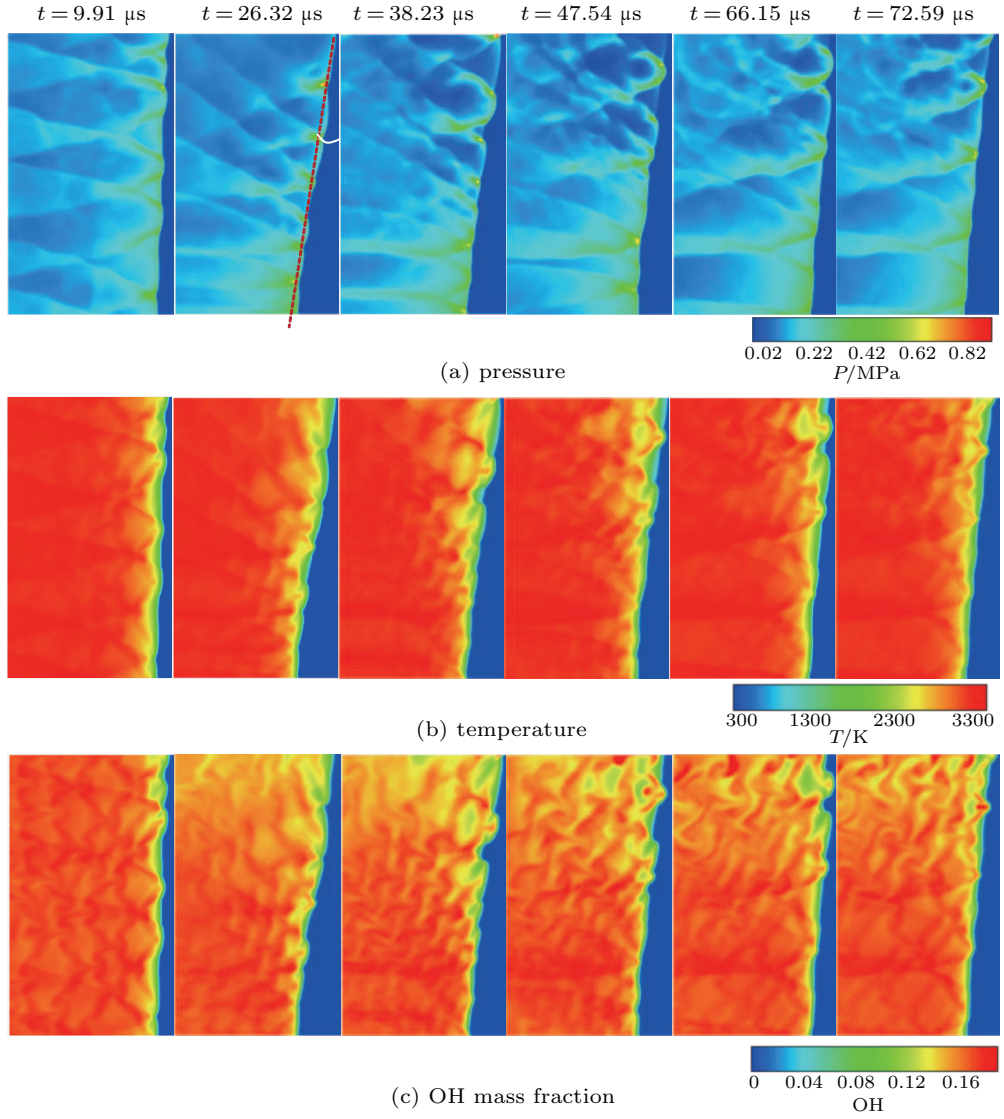


Fig. 3. Pressure, temperature, and OH mass fraction in the vicinity of distribution at different times for case 4.

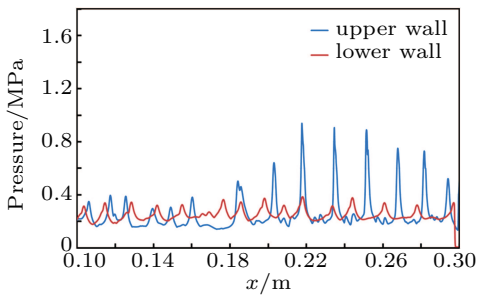


Fig. 4. Maximum pressure history on upper and lower walls for case 4.

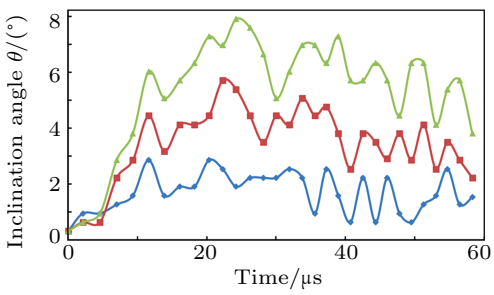


Fig. 5. Inclination angle of detonation front *versus* time for cases 2–4.

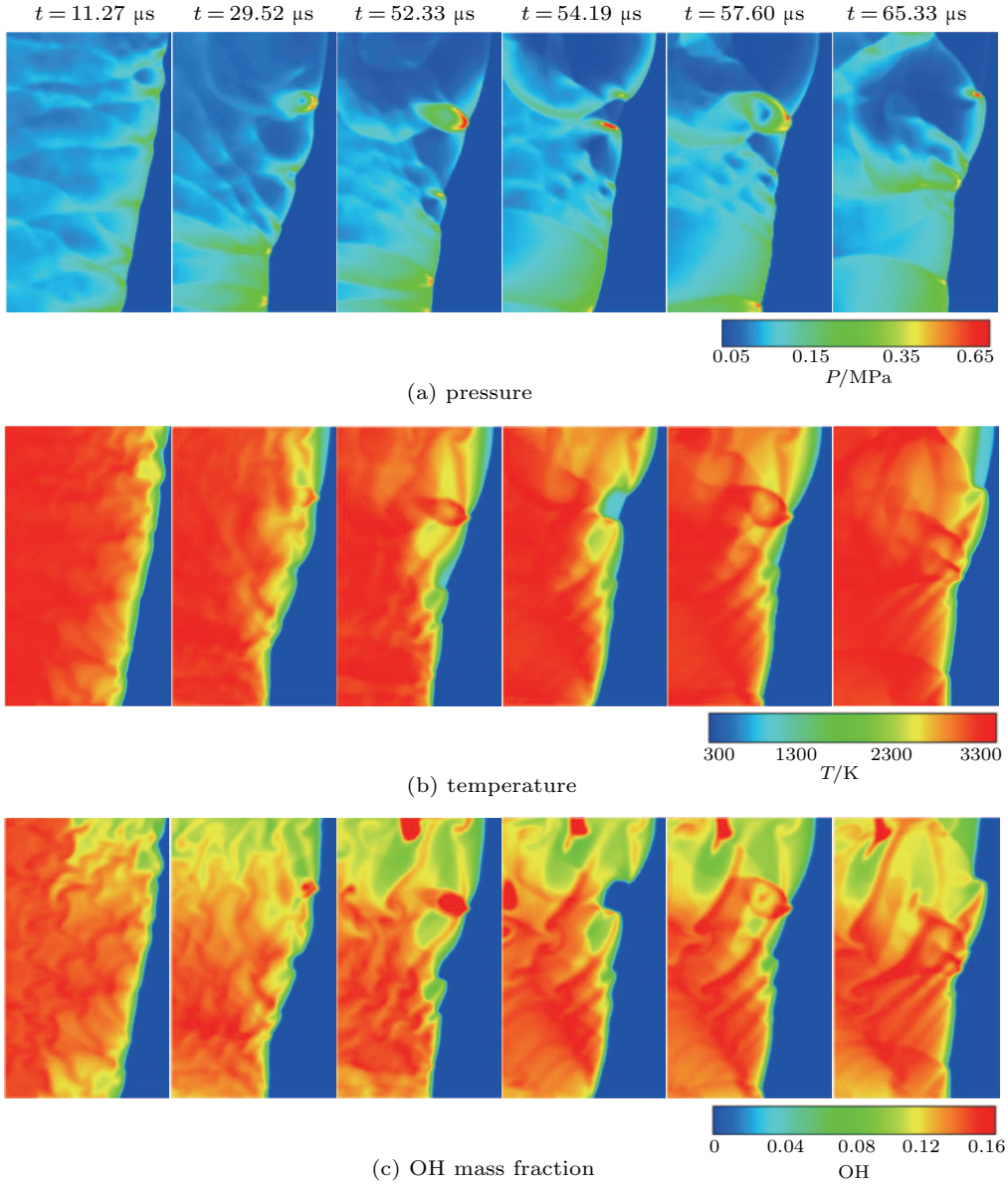


Fig. 6. Pressure, temperature, and OH mass fraction contours near the detonation front (case 6).

In summary, the increase of concentration gradient leads the cellular instability to globally increase. Overdriven detonation appearing in the fuel-rich layer near the upper wall can transport the energy into the fuel-lean layer by the triple-point collisions, which still sustains the detonation. Meanwhile, the triple points reduce into 6 less than that in the case 1.

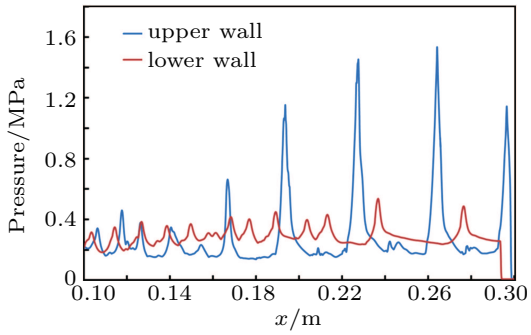


Fig. 7. Maximum pressure history at the upper and lower walls (case 6).

For the highly irregular detonation, the Mach stem produces a high temperature and pressure region in which the reaction tightly couples with the leading shock. Like the cases 4 and 6, the concentration gradient leads to the curved front and locally overdriven detonation in the fuel-rich layer near the upper wallas as shown in Fig. 8. It is found that at time $t = 21.04$ μs the Mach shock created by the strong and local explosion forms in the fuel-rich layer and fast runs forward with its strength decreasing, and sequentially recedes from the reaction layer at time $t = 35.54$ μs. Nevertheless, in the fuel-lean layer the detonation is very weak and even quenching detonation appears due to the lack of the fuel near the lower wall as shown in Figs. 8(a)–8(c). The triple points in the fuel-rich layer move to the fuel-lean layer and create the entropy-vortex rolls behind it, which also changes from 6 to 2. The entropy-vortex rolls can transport the fuel into the fuel-lean layer and

strongly local explosion occurs at the triple-shock intersection. Therefore, the transverse detonation forms, leading the detonation to be sustained. Figure 9 shows that the intense pressure pulse caused by the interaction of the local explosion wave with the wall appears at the upper wall, with a peak value of about ~ 1.6 MPa.

In summary, the triple point in the fuel-rich layer becomes strong and the global front is highly curved as the concentration gradient further increases to that in the case 9, while in the fuel-lean layer the detonation weakens and even quenches because here the mixture is close to detonation limit. The strong explosion in the cellular detonation in the fuel-rich layer plays a key role in initiating the fuel-lean detonation and sustaining globally the detonation.

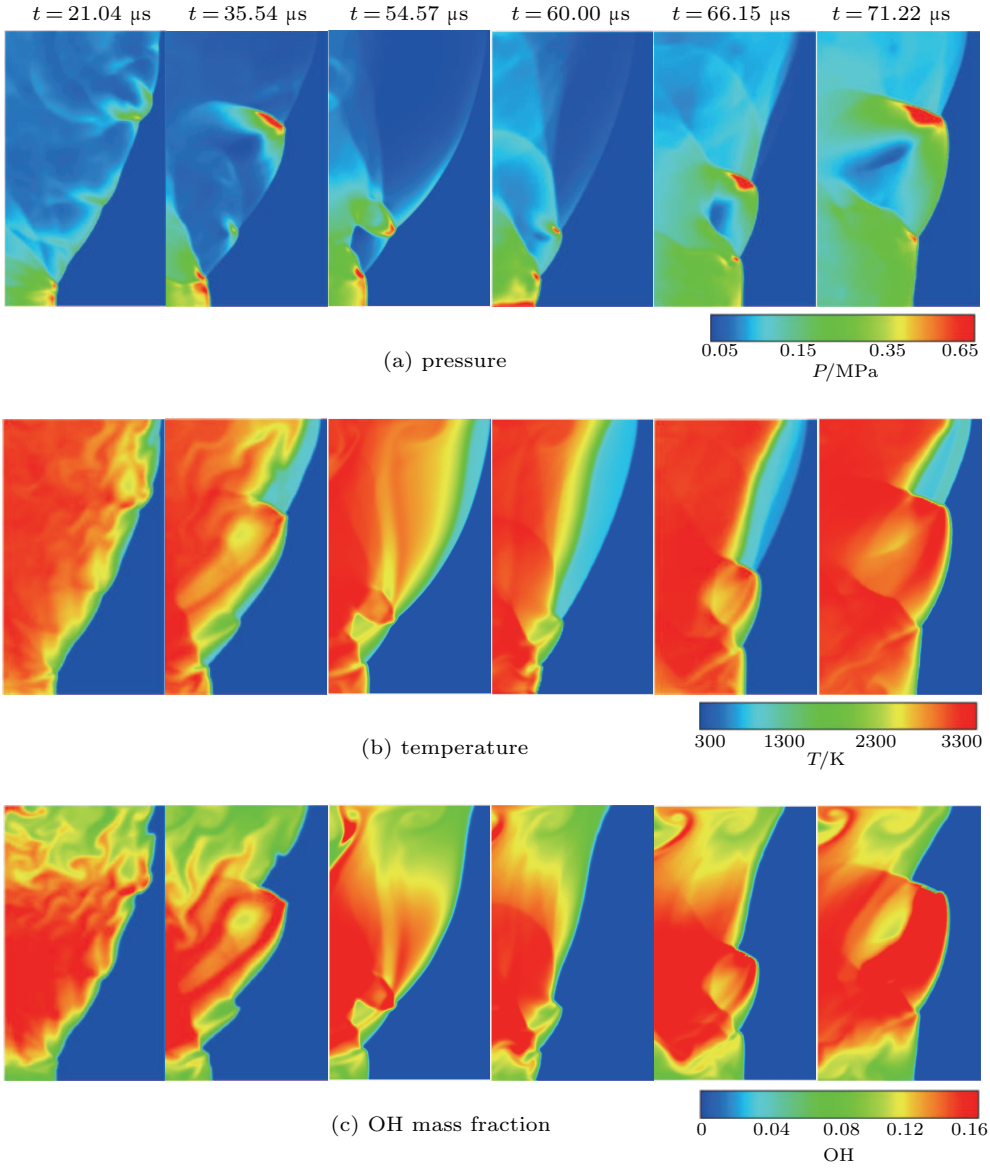


Fig. 8. Pressure, temperature, and OH mass fraction contours near detonation front (case 9).

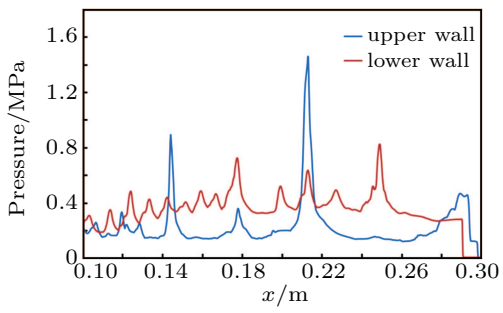


Fig. 9. Maximum pressure history at the upper and lower walls (case 9).

3.3. Cellular evolution at different concentration gradients

Figure 10 shows the initial evolutions of the cellular structure of detonation for different concentration gradients. It is seen that concentration gradient causes the cell pattern and regularity to change. For the cases 2–4, the cell is relatively regular, and the cell size in the fuel-rich layer is obviously larger than that in the fuel-lean layer. This influence becomes more obvious with the concentration gradient increasing. For

the cases 5 and 6, the cellular structure is globally more irregular and the front has large inclination angle. For the cases 8–11, globally the detonation cell becomes highly irregular and takes galloping behavior, which is also substantiated by the oscillating average detonation velocity in Figs. 12(g)–12(j), while in the fuel-lean layer near the lower wall the cellular detonation with low speed is sustained by the reflection of the triple point on the wall. For the cases 2–5, the detonations are globally stable and the cells are relatively uniform; eventually they propagate with the multi-head mode. For the cases 5–11, the non-uniform cellular detonations form at $x \approx 5$–20, and subsequent propagation mode is discussed below.

Figure 11 shows the long-time propagating modes of the detonation in the cases 7–11. It is seen that for the case 7 the detonation presents multi-head and a single-head mode alternately as shown in Fig. 11(a). For the cases 8–11, formed is a single-head mode with a periodic trajectory. This means that the detonation eventually propagates self-sustainingly. Furthermore, it is found that the cell periods are basically closed for different concentration gradients as shown in Figs. 11(b)–11(e). This is because the single-head detonation depends strongly on the boundary confinement. If the channel width is smaller than the cell size, the single-head mode usually appears and its period is determined by the channel width, depending on the concentration gradient. In the cases 8–11, the cell widths are larger than the channels width and hence the cells have the same period. It is worth noting that a bifurcation of the cell appears due to a local explosion as the gradient increases (see Figs. 11(c)–11(e)).

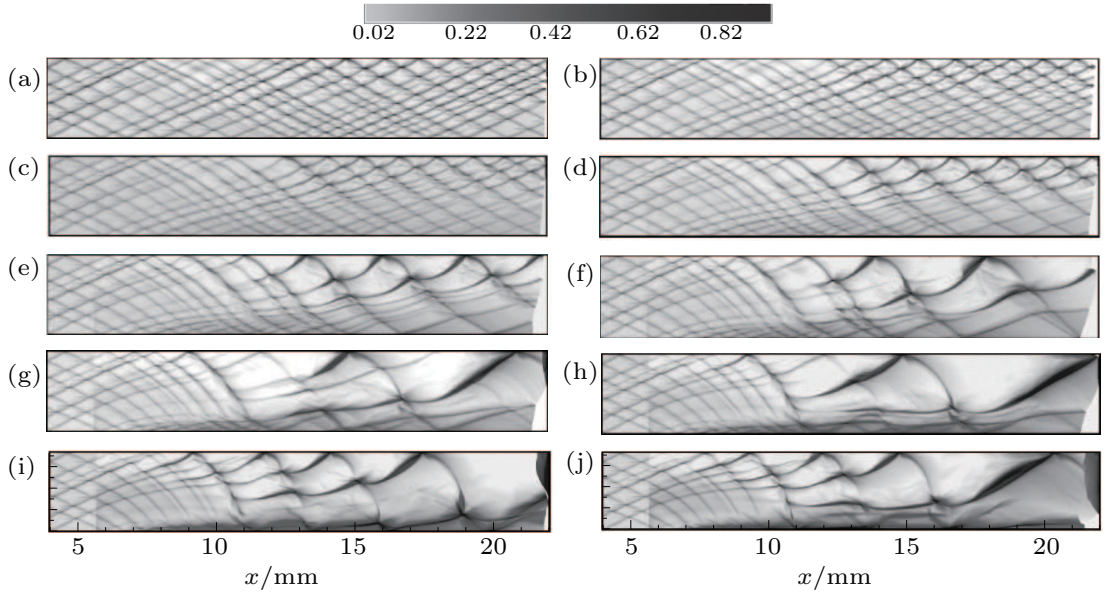


Fig. 10. Influences of concentration gradient on cellular structure of detonation wave: panels (a)–(j) are corresponding to cases 2–11 respectively.

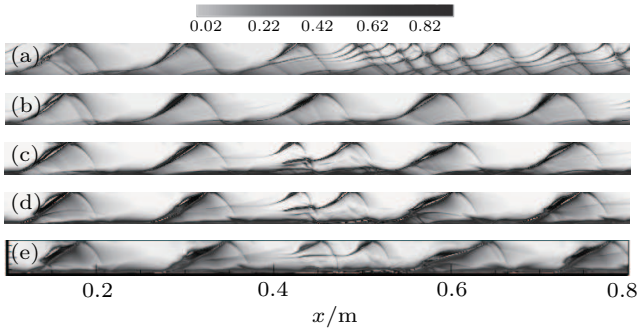


Fig. 11. Influences of the concentration gradient on cellular structure of the detonation wave. Panels (a)–(e) are corresponding to the cases 7–11 respectively.

In summary, when a single-head mode forms eventually, the detonation propagation is independent of the effect of the concentration gradient on cellular instability due to the confinement of the channel wall.

Figure 12 shows the propagating velocity of the detonations at the upper and lower walls for the cases 2–11. For the lower concentration gradient, the detonation velocity at the lower wall is nearly constant, while that at the upper wall takes slightly feather with a quasi-period oscillation. Globally, the average speed is basically the same as that in the uniform mixture. In the cases with higher concentration gradients, the amplitude of the oscillation increases while the period decreases, which are especially obvious for those of the upper wall shown in Figs. 12(a)–12(e). For the cases 8–11, the detonation velocity takes on low-frequency and high-amplitude pulsations at the upper wall, and the oscillation of the velocity at the lower wall also increases, demonstrating that the global detonation takes on a galloping propagation as shown in Figs. 10(g)–10(j) and 12(g)–12(j).

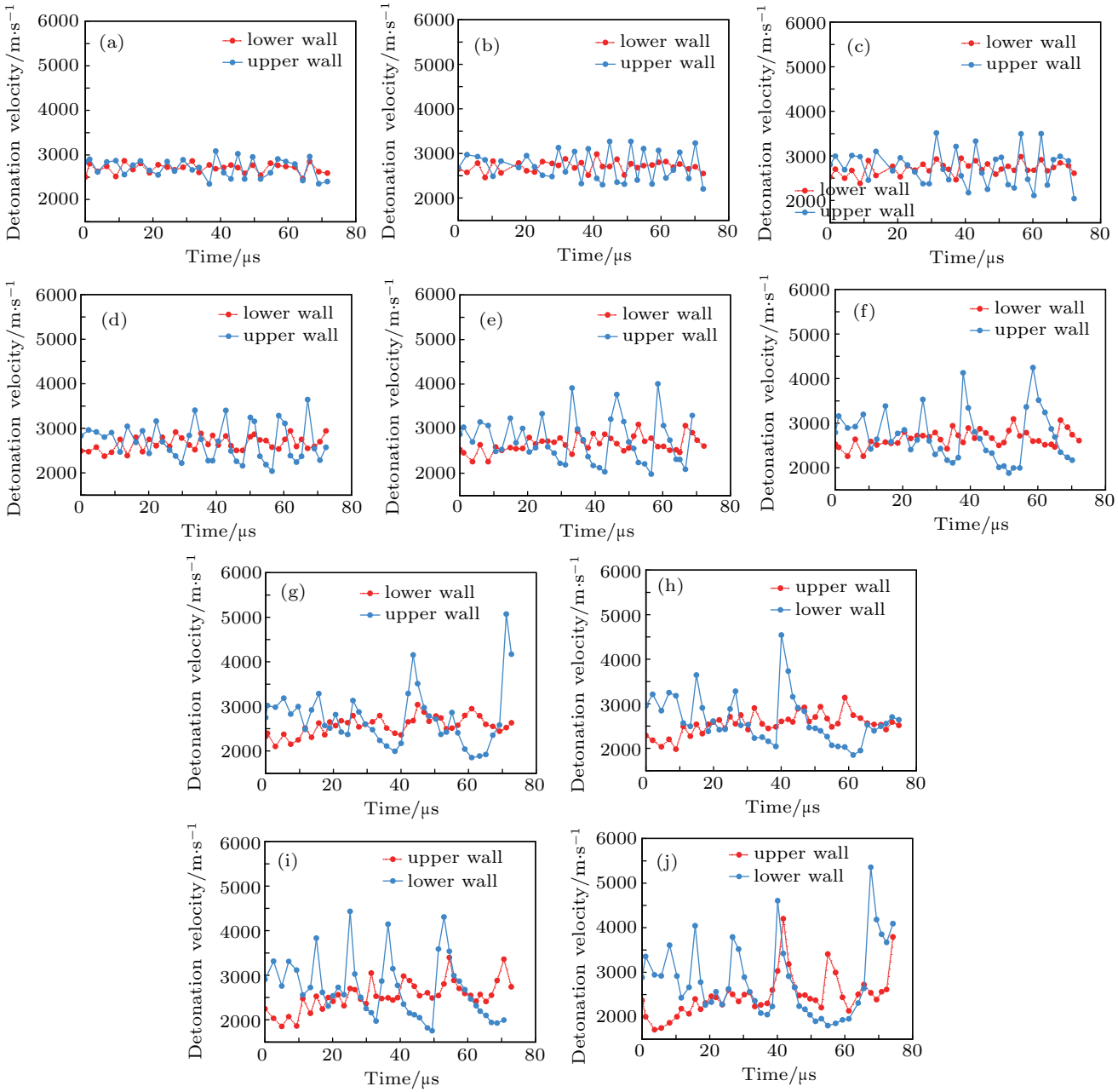


Fig. 12. Influences of concentration gradient on detonation velocity at upper and lower walls.

Table 2. Average detonation velocity at upper and lower walls.

Case	Upper wall	Lower wall
1	2820.04	2820.72
2	2817.28	2803.72
3	2841.32	2798.63
4	2806.18	2780.64
5	2821.30	2771.35
6	2832.24	2764.84
7	2812.86	2710.09
8	2827.82	2689.27
9	2752.05	2649.47
10	2798.75	2635.61
11	2818.48	2561.67

Table 2 shows the average detonation velocities at the upper and lower walls. The average detonation velocities without the concentration gradient are $\sim$ 2820 m/s, which agree with the experimental value.[1] For the lower concentration gradients (cases 2–6), each average detonation velocity is nearly close to that in the uniform mixture, while for the higher concentration gradients (cases 7–11), the average velocity is $\sim$ 2752 m/s–2827 m/s at the upper wall and $\sim$ 2561 m/s–2710 m/s at the lower wall. While the average velocity at the upper wall is still close to that in the case without the concentration gradient, the global detonation speed is significantly lower than that in the uniform mixture. This is reasonable because the improvement of the cellular instability and globally galloping behavior led by increasing the concentration gradient make the average velocity decrease.

3.4. Effect of channel width on detonation with concentration gradient

By the above discussion, it is demonstrated that the detonation propagation is eventually no longer affected by the variation of concentration gradient as it increases a certain value. This is because the boundary confinement plays a role in detonation propagation when it approaches to a detonation limit. Consequently, it is necessary to assess the role of the wall confinement in the detonation in the mixture with transversal concentration gradient. We take case 7 to carry out the simulation of a detonation in the channel of 72 mm, with $p_0 = 6.67$ kPa and $T_0 = 300$ K.

It is seen from Fig. 13 that the cell structure is highly irregular for the detonation propagating in the non-homogeneous gas, and differs from those in cases 7–11. One cell is shaped and the cell structure significantly differs from that in the channel of 36 mm. However, its cell period is larger than that in each of cases 7–11, which implies a weaker detonation as the confinement decreases. The intensity of transverse waves weakens significantly in the fuel-rich layer and their reflections have a weaker effect on the detonation propagation in the fuel-lean layer.

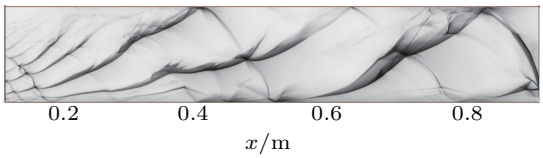


Fig. 13. The cellular structure of detonation happening in channel ($d = 72$ mm).

Figure 14 shows the history of shock pressure along the upper and lower wall for $d = 72$ mm. It is seen that the pressure oscillation along the upper wall takes on a mild amplitude which has a peak value of only ~ 0.58 MPa far less than ~ 1.55 MPa, while the large amplitude is ~ 0.75 MPa and it shows a low-frequency pressure pulse at the lower wall. This difference is also caused by the increase of the channel width.

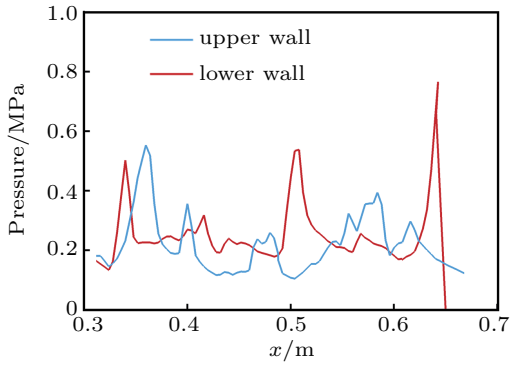


Fig. 14. The maaximum pressure history at upper and lower walls ($d = 72$ mm).

Figure 15 shows the typical pressure, the temperature, and the OH mass fraction contours at different times as the detonation cell forms. At $t = 103.06$ μs, the detonation front inclines obviously, with four triple points and the Mach stem appearing (see Fig. 15(a)). There is a small OH mass fraction near the fuel-rich layer, indicating the unreacted pockets behind the detonation front. It is also observed that OH mass fraction behind the Mach shock is low but higher at the triple points. Meanwhile, R–M and K–H instabilities at the boundary of the pocket generate small vortices, which promote burning the unreacted matter.

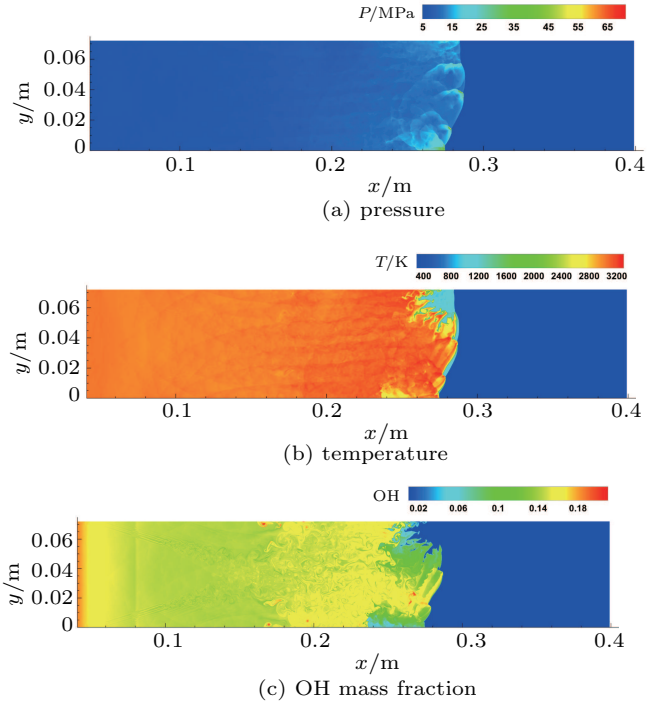


Fig. 15. Pressure, temperature, and OH mass fraction contours ($d = 72$ mm): $t = 103.06$ μs.

In summary, the detonation with the transversal concentration gradient depends strongly on the channel width and the confinement. The reason is that a wider channel provides a sufficient space for a wider range of the gas mixture, leading to a weaker shock as well as a reflection wave near the upper and lower boundaries, which effectively weakens the confinement. Finally, it can be concluded that a wider channel allows an unreacted pocket to be formed much more easily with a larger size than narrower channel. Therefore, according to the above, the detonation behaviors between narrow channel and the wide channel are different from each other substantionally.

4. Conclusions and perspectives

The third-order additive Runge–Kutta method, coupling the 5th-order WENO scheme is used to develop a high-resolution code for simulating the behavior of the detonation propagation in the H_2–O_2 mixture with the concentration gradient. By discussing the effects of the concentration gradient on the propagating mechanism and velocity, some conclusions are draw below.

(i) The concentration gradient enhances mainly the cellular instability. The detonation takes on relatively regular cell

for low gradient, and mildly irregular cell for mediate gradient, and highly irregular cell for large concentration gradient. The different shocked combustion modes appear in the rich-fuel and poor-fuel layer due to the concentration gradient effect. Globally, for the lower concentration gradients, the detonation is maintained by collision of triple points, while with the increase of the concentration gradient the detonation is sustained by strongly local explosion caused by the triple shock moving to the fuel-rich layer.

(ii) The high concentration gradient increases the cellular instability and causes globally a galloping propagation and hence the average detonation velocity is significantly lower than that in the uniform mixture, with the velocity oscillating obviously. When detonation propagation takes galloping behavior, the effect of concentration gradient on cellular instability can be ignored.

Appendix A: Verification of relative grid resolution

Case 11 is selected to be simulated with $\delta x = 5 \times 10^{-6}$ m and the grid convergence is verified. With mesh refining, the global features of the detonation tend to be consistent, with minor difference in the fine structure. The shock pressure along the middle line of the channel indicates quantitatively that the result with $\delta x = 1 \times 10^{-5}$ m is valid. At the same time, the detonation frontal structures are consistent for these two levels of grid resolution, as shown in Fig. A1. It can be shown that with mesh refining the global features of the detonation tend to be consistent, with minor difference in the fine structures. Consequently, the gird resolution of $\delta x = 1 \times 10^{-5}$ m is sufficient to capture the main feature of the single-head detonation with the steeper gradient.

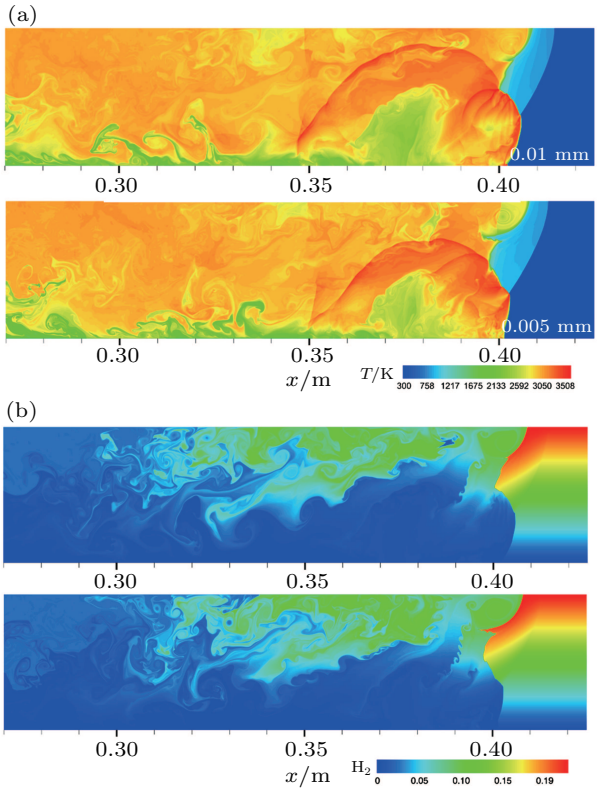


Fig. A1. Detonation front structure for case 11 ($t = 202.25$ μs).

References

[1] Liu J C, Liou J J, Sichel M, Kauffman C W and Nicholls J A 1988 21*th Symposium (International) on Combustion*, August 3–8, 1988, Technical University of Munich West Germany, Munich, Germany, pp. 1639–1647

[2] Short M and Sharpe G J 2003 *Combust. Thoer. Model.* **7** 401

[3] Short M 2001 *J. Fluid Mech.* **430** 381

[4] Ng H D, Radulescu M I, Higgins A J, Nikiforakis N and Lee J H S 2005 *Combust. Theor. Model.* **9** 385

[5] Zhang B, Liu H, Yan B J and Ng H D 2020 *Fuel* **259** 116220

[6] Zhang B 2019 *Fuel* **253** 305

[7] Zhang B and Liu H 2019 *Fuel* **258** 116132

[8] Lieberman D H and Shepherd J E 2007 *Shock Waves* **16** 421

[9] Bull D C, Elsworth J E, McLeod M A and Hughes D 1981 *Prog. Astronaut. Aeronaut.* **75** 61

[10] Donato M, Donato L and Lee J H 1981 *Proceedings of the First Specialists Meeting of the Combustion Institute*, July 20–25, 1981, Bordeaux, France

[11] Li J, Lai W H, Chung K and Lu F K 2008 *Combust. Flame* **154** 331

[12] Ishii K and Kojima M 2007 *Shock Waves* **17** 95

[13] Thomas G O, Sutton P and Edwards D H 1991 *Combust. Flame* **84** 312

[14] Vidal P 2009 *Int. J. Spray Combust* **1** 435

[15] Oran E S, Jones D A and Sichel M 1992 *P. Roy. Soc. A-Math. Phys.* **436** 267

[16] Vollmer K G, Ettner F and Sattelmayer T 2012 *Combust. Sci. Technol.* **184** 1903

[17] Kessler D A, Gamezo V N and Oran E S 2011 *Proceedings of the* 23*th International Colloquium on the Dynamics of Explosions and Reacting Systems*, July 24–29, 2011, Irvine, California, USA

[18] Boeck L R, Berger F M, Hasslberger J and Settalmayer T 2016 *Shock Waves* **26** 181

[19] Ishii K and Kojima M 2007 *Shock Waves* **1** 795

[20] Calhoon W H Jr and Sinha N 2005 43*rd AIAA Aerospace Sciences Meeting and Exhibit*, January 10–13, 2005, Reno, Navada, USA, pp. 42–43

[21] Kessler D A, Gamezo V N and Oran E S 2011 *Proc. Roy. Soc. A-Math. Phys.* **370** 567

[22] Ettner F, Vollmer K G and Sattelmayer T 2010 *Proceedings of the* 8*th International Symposium on Hazards, Prevention and Mitigation of Industrial Explosions*, September 5–10, 2010, Yokohama, Japan

[23] Berets D J, Greene E F and Kistiakowsky G B 1950 *J. Am. Chem. Soc.* **72** 1080

[24] Engebretsen T, Bjerketvedt D and Sonju O K 1992 *Prog. Astronaut. Aeronaut.* **153** 324

[25] Kuznetsov M S, Dorofeev S B, Efimenko A A, Alekseev V I and Breitung W 1997 *Shock Waves* **7** 297

[26] Kuznetsov M, Alekseev V I, Dorofeev S, Matsukov I D and Boccio J L 1998 *P. Combust. Inst.* **27** 2241

[27] Qu Q, Khoo B C, Dou H S and Tsai H M 2008 *Shock Waves* **18** 213

[28] Sánchez A L and Williams F A 2014 *Prog. Energy Combust. Sci.* **41** 1

[29] Sochet I, Lamy T and Brossard J 2000 *Shock Waves* **10** 363

[30] Sánchez A L and Williams F A 2014 *Prog. Energy Combust. Sci.* **41** 1

[31] Tonello N A, Sichel M and Kauffman C W 1995 *Shock Waves* **5** 225

[32] Huang J, Han W H, Gao X Y and Wang C 2019 *Chin. Phys. B* **28** 074704

[33] Austin J M, Pintgen F and Shepherd J E 2004 42*nd AIAA Aerospace Sciences Meeting and Exhibit*, January 5–8, 2004, Reno, Nevada